

UC Office of the President

Recent Work

Title

An efficient measure of compactness for two-dimensional shapes and its application in regionalization problems

Permalink

<https://escholarship.org/uc/item/4zx6s12s>

Journal

International Journal of Geographical Information Science, 27(6)

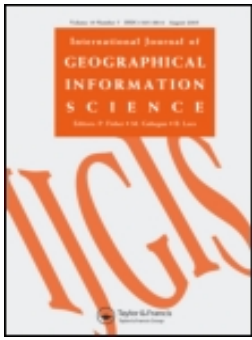
Authors

Li, Wenwen
Goodchild, Michael F
Church, Richard

Publication Date

2013-01-22

Peer reviewed



An efficient measure of compactness for two-dimensional shapes and its application in regionalization problems

Wenwen Li , Michael F. Goodchild & Richard Church

To cite this article: Wenwen Li , Michael F. Goodchild & Richard Church (2013) An efficient measure of compactness for two-dimensional shapes and its application in regionalization problems, International Journal of Geographical Information Science, 27:6, 1227-1250, DOI: 10.1080/13658816.2012.752093

To link to this article: <http://dx.doi.org/10.1080/13658816.2012.752093>



Published online: 22 Jan 2013.



Submit your article to this journal [↗](#)



Article views: 565



View related articles [↗](#)



Citing articles: 22 View citing articles [↗](#)

An efficient measure of compactness for two-dimensional shapes and its application in regionalization problems

Wenwen Li^{a*}, Michael F. Goodchild^b and Richard Church^b

^a*School of Geographical Sciences and Urban Planning, GeoDa Center for Geospatial Analysis and Computation, Arizona State University, Tempe, AZ, USA;* ^b*Department of Geography, University of California, Santa Barbara, CA, USA*

(Received 4 July 2012; final version received 9 November 2012)

A measure of shape compactness is a numerical quantity representing the degree to which a shape is compact. Ways to provide an accurate measure have been given great attention due to its application in a broad range of GIS problems, such as detecting clustering patterns from remote-sensing images, understanding urban sprawl, and redrawing electoral districts to avoid gerrymandering. In this article, we propose an effective and efficient approach to computing shape compactness based on the moment of inertia (MI), a well-known concept in physics. The mathematical framework and the computer implementation for both raster and vector models are discussed in detail. In addition to computing compactness for a single shape, we propose a computational method that is capable of calculating the variations in compactness as a shape grows or shrinks, which is a typical application found in regionalization problems. We conducted a number of experiments that demonstrate the superiority of the MI over the popular isoperimetric quotient approach in terms of (1) computational efficiency; (2) tolerance of positional uncertainty and irregular boundaries; (3) ability to handle shapes with holes and multiple parts; and (4) applicability and efficacy in districting/zonation/regionalization problems.

Keywords: moment of inertia; compactness; shape analysis; regionalization; districting; shape index; automated zoning procedure; pattern recognition; geographic Information Science; vector data modelling; raster data modelling

1. Introduction

The compactness measure of a shape, also known as its shape index, is a numerical quantity representing the degree to which a shape is compact (Gillman 2002). Here, shape refers to geometric objects that have a two-dimensional extent, such as objects used to describe a park or a parcel of land, as opposed to one-dimensional features such as network links or three-dimensional features such as a globe. Compactness is acknowledged as one of the most intriguing and important properties of a shape (Angel *et al.* 2010) and is widely used as a descriptor in a variety of domain tasks. For instance, compactness is a critical factor in defining and analyzing homogeneous habitat regions in ecology (Eason 1992). Within computer vision, there have been many applications of shape compactness for object matching and pattern recognition (Edwards *et al.* 2003). In content-based image

*Corresponding author. Email: wenwen@asu.edu

retrieval, this factor is used to identify shape signatures for non-rigid shape search and retrieval in large databases (Ovsjanikov *et al.* 2009). In psychological studies, compactness has been introduced to quantify perceptual stability and to understand the causes of perceived shape aesthetics (Friedenberg 2012).

In GIScience, the quantification and computation of shape compactness has been a long-standing and fundamental research question for a number of reasons. First, a compact region has appealing properties because compactness implies maximum accessibility to all parts of the shape, and a compact shape is likely to be homogeneous, therefore sharing common attributes and properties (Tobler 1970). Second, identification of shape has a great impact on the search for, and extraction of, spatial patterns, which is essential to analyzing and understanding geographical phenomena, as well as predicting future patterns (Wentz 1997). Third, the geographical world is populated with spatial objects described through areal representations, making compactness an important part of understanding these objects. Therefore, shape comparison has been given great attention due to its application in a broad range of geographical problems (MacEachren 1985). For example, there has been a long history of using compactness within political geography to assess the constitutionality of political districts based on their shape (Gibbs 1961, Rinder *et al.* 1988, Fryer and Holden 2007). In urban morphology studies, Christaller (1968) deduced the emergence of compact hexagonal arrangements of towns in his 'central place theory' (CPT). More recently, compactness has become a well-established principle used to guide city planning, evaluate urban settings, and study urban sprawl (Chandra *et al.* 2009). In addition, compactness is a well-known index to describe the hydrological properties of drainage basins (Bardossy and Schmidt 2002).

The geospatial applications mentioned above concern the role of compactness as a shape index to measure a *single* shape. In practice though, there are also a significant number of applications requiring the computation of compactness for two or more adjacent shapes that are grouped together. This type of application, called *regionalization*, often involves large spatial datasets, such as census data, and requires the aggregation of a large number of shapes into a smaller number of larger regions. Using compactness as a measure in regionalization was discussed as early as the 1960s; Weaver and Hess (1963) emphasized the importance of generating compact regions in designing political districts. Kaiser (1966) and Young (1988) discussed the use of moment of inertia conceptually in measuring the compactness of electoral districts and concluded that moment of inertia is not only good at measuring compactness, but also provides a measure of size. In 1977, Openshaw discussed the importance of achieving a degree of compactness in solving the Modifiable Areal Unit Problem (MAUP) (Openshaw 1977, 1978). In 1995, Openshaw and Raw discussed Automatic Zoning Procedure (AZP) for census redesign, which became the basis for the design of the 2001 UK census geography (Martin *et al.* 2001). In this procedure, compactness was considered to be an important requirement to meet. Since then, many compactness measures have been proposed by the geography community (Horn *et al.* 1993), such as those based upon isoperimetric quotients, reference shape comparison, and moment of inertia. There are also a number of indirect compactness measurements, such as methods based on the distance to a reference point (Hauert and Wolf 2010), ratio of the actual area of a region to its minimum external peripheral area (Datta *et al.* 2012), and those reviewed by Duque *et al.* (2007).

To evaluate the efficiency and effectiveness of compactness measures, we propose the following criteria: (1) robust, (2) computationally efficient, and (3) additive. Robust here meaning the algorithm should be able to measure the compactness of any shape. As any

digitization process produces some degrees of uncertainty (Goodchild 1996), a robust measure should also be relatively insensitive to such uncertainty. Moreover, a robust measure should be stable for a given fixed shape regardless of changes in size and spatial resolution. In addition to robustness, computational efficiency is an important factor when problem sizes are very large. A good algorithm for computing compactness should be computationally efficient to the extent that it is not a bottleneck in GIS processing. In addition, for some practical applications such as a regionalization problem, one may need to measure the changing compactness of a region as it is combined with other areas on the fly, instead of recomputing compactness from scratch at each iteration. In fact, an algorithm should be able to obtain a compactness value when merging two or more regions using a simple summation approach; in other words, the algorithm should be ‘additive’, which is the third criterion. A compactness measurement approach that is additive and easy to compute will reduce computational complexity and improve the computational efficiency and effectiveness when used in real-world applications.

In this article, we propose a new and efficient way to compute compactness based on the concept of the moment of inertia (MI), a well-known quantity in physics. Although earlier research has considered the use of MI (Kaiser 1966, Massam and Goodchild 1971, Zhang *et al.* 2006), considerable barriers existed in its widespread adoption. First, there was no clear, definable way in which it could be applied. Second, few tests have demonstrated its superiority. We therefore attempt to address both of these barriers. Section 2 reviews the existing methods for computing compactness and their pros and cons. Section 3 discusses in detail the mathematical equations of our proposed trapezium-based method for computing moment of inertia for both vector and raster data. Section 4 provides details of how this approach can be implemented. Section 5 compares statistically the performance of our proposed method against the commonly used Iso-Perimetric Quotient (IPQ) measure. Section 6 introduces a large practical application of this method in generating a set of 100 compact zones spanning Southern California that are used as the basic spatial units for a large scale economic simulation model. Section 7 concludes the work and proposes directions for future research.

2. Literature review

There is a long history of interest in the science community in developing an effective compactness measure; in 1822, Ritter proposed to measure a shape’s compactness using a simple ratio of the perimeter (P) to the area (A) of the shape (Frolov 1975). Since then, a variety of compactness measures have been proposed (Miller 1953; Richardson 1961, Cole 1964, Massam and Goodchild 1971, Frolov 1975, Osserman 1978, Kim and Anderson 1984, Bribiesca 1997, Bachi 1999, Bottema 2000, Wentz 2000, Zhao and Stough 2005, Santiago and Bribiesca 2009). These measures can be grouped into four categories: area–perimeter measurement, reference shape, geometric pixel properties, and dispersion of elements of area.

The method (P/A) proposed by Ritter can be categorized as an area–perimeter approach. Although straightforward, Ritter’s simplistic ratio suffers from the fact that the measure varies when shape size changes. To account for this limitation, the measure can be made dimensionless by dividing the shape’s area by the square of its perimeter. Among many alternative names and precise mathematical forms that have been given to this class of metrics, including the circularity ratio $4A/P^2$ by Miller (1953) and the compactness ratio $2\sqrt{\pi}A/P$ by Richardson (1961), the IPQ (Osserman 1978) has become one of the most widely accepted compactness measures of this class. It is defined as:

$$C_{IPQ} = \frac{4\pi A}{P^2} \quad (1)$$

where the perimeter P is squared to remove the scaling effect, A is the area of the shape, and C_{IPQ} is the compactness value. By adding π in the numerator of Miller's circularity ratio, C_{IPQ} 's range is changed to $(0, 1]$ (instead of 0 to $1/\pi$ in Miller's measure). A shape with a high value of C_{IPQ} is considered to be more compact than a shape with a lower C_{IPQ} . A circle is the most compact shape, and by definition above, it will have a compactness value of 1. This measure is also the square of Richardson's compactness ratio. Although the IPQ approach is not very stable for irregular contours (Santiago and Bribiesca 2009), it is applicable in computing the compactness index for both vector and raster data, it is easy to compute, and it is not sensitive to size changes (keeping shape constant). Therefore, it remains the most popular shape index to date (Santiago and Bribiesca 2009).

Another approach to the measurement of compactness uses reference shapes. For instance, Cole (1964) proposed a compactness measure to compare the area of a shape, A , with the area of the smallest circle that circumscribes the shape, A_{sc} . This is an alternative form of Gibbs's (1961) compactness measure $4A/L^2$, where L is the longest line between two points on a shape's perimeter. Kim and Anderson (1984) later termed this the digital compactness measure (DCM). DCM is defined as:

$$C_{DCM} = \frac{A}{A_{sc}} \quad (2)$$

Like the IPQ, its maximum value, 1, will occur when the shape is a circle. The major drawbacks of this method are that it cannot be applied to shapes with holes, it is not additive and scale-invariant. A second approach that falls in this category was proposed by Bottema (2000). It works by overlaying the shape S with a circle C of the same area and computing the overlap. Suppose the area of S is A , and the area of C is A_0 , then Bottema's compactness measure can be expressed as:

$$C_{Bottema} = 1 - \frac{|A \cap A_0|}{A_0} \quad (3)$$

Another alternative index falling in this category is the elongation index (Wentz 2000), which is a type of overlap index (Zhao and Stough 2005) that sets a condition of equal-area matching. It is calculated from the ratio of maximum overlap of the intersection to the union of the object with a circle of equal area. Mathematically,

$$EI = \frac{|A \cap A_0|}{|A \cup A_0|} \quad (4)$$

A and A_0 hold the same meanings as in Equation (3). The overlap could also be determined by coinciding the centroids of the shape and the reference shape (Zhao and Stough 2005). Both the Bottema measure and the elongation index are capable of measuring compactness of a shape with holes; however, like the DCM method, they are sensitive to size changes in computation. Moreover, the circle can be overlaid on the shape in many different positions, so a search must be invoked to determine the position of maximum overlap, making this type of method less competitive from a computational perspective.

Other shape-reference approaches include the comparison of the area or diameter of the maximum inscribed circle to that of the minimum circumscribed circle. The approaches in this category have common drawbacks. First, the parameter is difficult to measure; for example, for Bottema's approach, there must be a procedure to compute the intersection of two areas. Second, the compactness of a shape is not computable from its parts; when this measure is used in a regionalization process, the compactness of a given region must be recalculated every time it grows or shrinks. These drawbacks make the shape reference approach less appealing in practical applications.

The third category is designed to work on raster datasets. A representative method of this class of methods is called the normalized discrete compactness (NDC) measure, suggested by Bribiesca (1997). The idea is to count the number of cell sides (L_D) shared between pixels that represent a shape S , and then calculate the measure C_{NDC} . This is given as:

$$C_{\text{NDC}} = \frac{L_D - L_{D_{\min}}}{L_{D_{\max}} - L_{D_{\min}}} \quad (5)$$

where $L_{D_{\min}}$ and $L_{D_{\max}}$ are the lower and upper limits of the number of cell sides that can be shared with the same number of pixels within S . Defining p as the number of edges on the border and n as the total number of pixels in S , L_D , $L_{D_{\min}}$, and $L_{D_{\max}}$ can be obtained from Equations (6)–(8):

$$L_D = \frac{4n - p}{2} \quad (6)$$

$$L_{D_{\min}} = n - 1 \quad (7)$$

$$L_{D_{\max}} = 2(n - \sqrt{n}) \quad (8)$$

The NDC approach has the advantage of being scale invariant, and can be applied when computing the compactness of shapes with holes.

The last category of measures is based on analyzing the dispersion of elements/components in a shape. This approach involves the calculation of the second moment of an area about a point, also known as the moment of inertia (MI). According to Massam and Goodchild (1971), each shape can be considered as composed of infinitesimally small units of area da , and the MI of a shape is defined as the second moment of an area about a point s on the shape as follows:

$$I_s = \int z^2 da \quad (9)$$

where z is the distance from da to s . Similarly, the MI about its centroid can be defined as:

$$I_g = \int z_g^2 da \quad (10)$$

where z_g is the distance from da to the centroid of a shape. 'The moment about a point s ' means the moment about an axis perpendicular to the shape through the point s ; we use the former phrase throughout the article for simplicity. The 'centroid' in GIS has come to mean any point representative of a shape, but it is used here in its strict mathematical

sense as the balance point and the point about which the MI is minimum for any shape. The shape index base upon MI, C_{MI} , is calculated as the ratio of the MI of a circle of the same area about its center, to the MI of the shape about its centroid. The value range of C_{MI} is (0,1]; larger values means more compact shape. A circle receives the maximal value of 1. Mathematically, it can be expressed as:

$$C_{MI} = \frac{A^2}{2\pi I_g} \quad (11)$$

where A is the area of a shape. Bachi (1999) reviewed this measure and some equivalent measures. This measure is readily additive, since the index for an aggregate of shapes is easily computed from the relevant properties of each component shape, as we will show below. The measure is also insensitive to shape size and rough boundaries. This approach is also appealing due to its ability in distinguishing between the shape of the region being measured and the shape of a specific distribution of sub-regions within the region. Therefore, it has extensive applicability in a regionalization problem.

In Massam and Goodchild's (1971) implementation, the primitive elements used to represent the shape, da , were triangles. However, there is no simple, obvious, and robust way to divide a polygon into triangles uniquely. To our best knowledge, there are no specific discussions in the literature on how to compute the MI of a shape efficiently. To overcome this limitation, in Section 3 we propose a trapezium-based approach which provides an efficient and unique alternative to measuring MI-based compactness. We also discuss how to handle shapes with multiple parts and shapes with holes, as well as how this approach can be further simplified when applied to a raster.

3. Methods for computing the centroid and moment of inertia

3.1. Moment of inertia of a single shape

To compute the compactness C_{MI} of a shape we must first compute the coordinates (x_g^i, y_g^i) of the centroid g :

$$x_g^i = \frac{\int x da_i}{a_i}, y_g^i = \frac{\int y da_i}{a_i} \quad (12)$$

where x and y are the coordinates of da_i and a_i is the area's measure. To compute these properties, we represent the area as a polygon and partition the polygon into primitive elements using trapezia. Figure 1 shows a polygon defined as a clockwise sequence of n vertices $(x_1, y_1), (x_2, y_2), \dots, (x_n, y_n)$, and define $(x_{n+1}, y_{n+1}) = (x_1, y_1)$. For any adjacent pair of vertices, drop perpendiculars to the x -axis. Taking the segment with endpoints (x_i, y_i) and (x_{i+1}, y_{i+1}) as an example, when dropping perpendiculars to the x -axis, a trapezium is formed with two vertical sides, one horizontal side, and one diagonal side. The calculation of moment of inertia of the trapezium T_i formed from segment with endpoints (x_i, y_i) and (x_{i+1}, y_{i+1}) , about its centroid, can be reduced to calculating the composition of the moments for the triangle piece (T) and the rectangle piece (R) about their respective centroids, and then combining them appropriately. For the triangle piece,

$$a_{i_T} = (x_{i+1} - x_i)(y_{i+1} - y_i)/2 \quad (13)$$

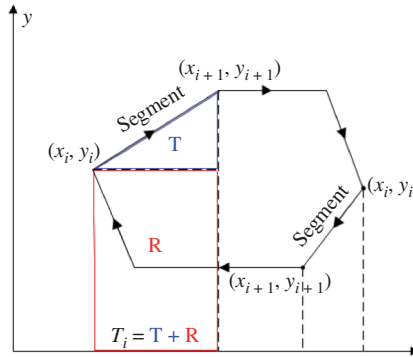


Figure 1. A polygon with points defined clockwise, showing the trapezia generated from two of its segments.

$$x_{g_T}^i = (x_i + 2x_{i+1}) / 3 \tag{14}$$

$$y_{g_T}^i = (2y_i + y_{i+1}) / 3 \tag{15}$$

$$I_{i_T} = a_{i_T} [(x_{i+1} - x_i)^2 + (y_{i+1} - y_i)^2] / 18 \tag{16}$$

For the rectangle piece,

$$a_{i_R} = (x_{i+1} - x_i)y_i \tag{17}$$

$$x_{g_R}^i = (x_i + x_{i+1}) / 2 \tag{18}$$

$$y_{g_R}^i = y_i / 2 \tag{19}$$

$$I_{i_R} = a_{i_R} [(x_{i+1} - x_i)^2 + y_i^2] / 12 \tag{20}$$

where a_i denotes area, (x_g^i, y_g^i) is the centroid, and I_i denotes the MI of each piece. Note that for any piece falling below or completely outside of the polygon, the values for a_{i_T} and a_{i_R} will be negative. For example, when computing the area of the rectangle piece of the trapezium associated with the segment on the lower right portion of the polygon, x_i exceeds the value of x_{i+1} , the difference $x_{i+1} - x_i$ will be negative, and thus the area calculated in Equation (17) will be negative in value.

The calculation of MI for the whole polygonal area requires combining all triangle and rectangle pieces. The total polygon area, A , can be obtained by adding the areas of triangle and rectangle pieces with respect to sign. Equation (21) presents the mathematical equation. The centroid of the polygon is obtained by averaging the coordinates of all vertices, as Equation (22) shows.

$$A = \sum_{i=1}^n (a_{i_T} + a_{i_R}) \tag{21}$$

$$x_g = \sum_{i=1}^n \frac{(x_{g,R}^i a_{i,R} + x_{g,T}^i a_{i,T})}{A}, \quad y_g = \sum_{i=1}^n \frac{(y_{g,R}^i a_{i,R} + y_{g,T}^i a_{i,T})}{A} \tag{22}$$

For computing the entire I_g of A, according to the parallel axis theorem (Landau and Lifschitz 1984), the MI about any point s is related to the MI about the centroid g by:

$$I_s = I_g + d^2 da \tag{23}$$

where d is the distance from the centroid to s . Adjusting the moments of inertia of all pieces to the polygon centroid yields I_g , illustrated in Equation (23):

$$I_g = \sum_{i=1}^n (I_{i,T} + d_{i,T,g}^2 A_{i,T} + I_{i,R} + d_{i,R,g}^2 A_{i,R}) \tag{24}$$

where $d_{i,T,g}$ and $d_{i,R,g}$ are the distances between the centroids of the triangle and rectangle pieces of trapezium i and the centroid of the polygon, respectively. Note that as the pieces falling below or completely outside of the polygon have a computed negative area, their moments are automatically subtracted from the total. Substituting I_g in Equation (11), the shape index (normalized MI) can be easily obtained. In summary, Equations (13)–(16) compute the area, centroid, and MI of the triangle piece of trapezium T_i formed from segment (x_i, y_i) to (x_{i+1}, y_{i+1}) . Equations (17)–(20) compute the area, centroid, and MI of the rectangle piece of the trapezium T_i . Equations (21)–(24) compute the area, centroid, and MI of the whole polygon by grouping all the triangle and rectangle pieces of the n trapezia formed by the n segments of the polygon.

3.2. Moment of inertia of a region

Section 3.1 introduced the computation of MI of a single shape. In the context of a regionalization problem, we also require the on-the-fly computation of MI as a region grows or shrinks based upon the addition or subtraction of polygonal spatial units. For instance, given a partial region P aggregated from a set of atomic units u_1, u_2, \dots, u_m and supposing that the area of P at current state j is $A_{p(j)}$, its MI is $I_{p(j)}$ and the centroid is $(x_g^{p(j)}, y_g^{p(j)})$. When a region P grows, this must involve the addition of another atomic unit u_k , which has the properties of area A_{u_k} , centroid (x_{g-u_k}, y_{g-u_k}) , and MI I_{u_k} . The compactness of P at new state $j + 1$ can be easily obtained by combining the properties of P in state j and that of the atomic unit as follows:

$$I_{p(j+1)} = I_{p(j)} + I_{u_k} + A_{p(j)} d_{p(j+1),p(j)}^2 + A_{u_k} d_{p(j+1),u_k}^2 \tag{25}$$

$$A_{p(j+1)} = A_{p(j)} + A_{u_k} \tag{26}$$

$$x_g^{p(j+1)} = (A_{p(j)} x_g^{p(j)} + A_{u_k} x_{g-u_k}) / A_{p(j+1)} \tag{27}$$

$$y_g^{p(j+1)} = (A_{p(j)} y_g^{p(j)} + A_{u_k} y_{g-u_k}) / A_{p(j+1)} \tag{28}$$

where $d_{p^{(j+1)}, p^{(j)}}$ refers to the distance between the centroid of region P at state j and the new centroid after attaching atomic unit u_k . We can also call the new centroid the centroid of P at state $j + 1$, and obtain it from Equations (27) and Equations (28). Equation (25) is the calculation of the moment of inertia for P at state $j + 1$. We can tell from this equation that the moment of inertia of a new region when combining two sub-regions equals the sum of the MI of both sub-regions and the increase caused by the merging. This calculation avoids the recomputation of compactness for all constitutional units, and therefore, is computationally efficient and additive. Equation (25) can also be used as the theoretical foundation for calculating the compactness of a shape with multiple parts (connected or otherwise).

Similarly, when a basic unit u_k is switched out of or removed from region P at state j , the properties of P at state $j + 1$ can be obtained from:

$$I_{p^{(j+1)}} = I_{p^{(j)}} - I_{u_k} - A_{p^{(j+1)}}d_{p^{(j+1)}, p^{(j)}}^2 - A_{u_k}d_{u_k, p^{(j)}}^2 \tag{29}$$

$$A_{p^{(j+1)}} = A_{p^{(j)}} - A_{u_k} \tag{30}$$

$$x_g^{p^{(j+1)}} = (A_{p^{(j)}}x_g^{p^{(j)}} - A_{u_k}x_{g-u_k})/A_{p^{(j+1)}} \tag{31}$$

$$y_g^{p^{(j+1)}} = (A_{p^{(j)}}y_g^{p^{(j)}} - A_{u_k}y_{g-u_k})/A_{p^{(j+1)}} \tag{32}$$

Equation (29) shows that when removing a sub-region, the MI not only decreases by that of the sub-region, but also by the loss in splitting, reflected in the centroid changes. This equation can also be used to calculate the compactness of a shape with holes.

Whenever the shape of a region is changed, the MI is recalculated. Then by substituting this value in Equation (11), the shape index (normalized MI) can be obtained.

In summary, Equations (25)–(28) compute the new MI, area, and centroid of a region after merging an atomic unit. Equations (29)–(32) compute the new MI, area, and centroid of a region after removing an atomic unit from it. The attributes (MI, area, and centroid) of an atomic unit used in Equations (25)–(32) are obtained from Equations (12)–(20). Rather than recomputing the MI of a region every time it changes, these equations provide a means of additively computing the MI and the shape index. This constitutes the building block for an efficient algorithm to be integrated into a compactness-driven regionalization problem.

3.3. *Computation of shape index on raster data models*

The proposed method has the advantage of being easily calculated from boundary coordinates. There is, however, a further simplification that can be made when using raster datasets. For a geo-referenced raster dataset, instead of using the coordinates of vertices to depict a shape (red region in Figure 2), the geographic extent (the top, bottom, left and right coordinates of a rectangle covering all of the raster dataset’s data) and the cell size (r) are employed. Each pixel can be identified by its row and column indices (s, t) in a rectangular matrix (M). In order to integrate the MI measure of a raster dataset into our current methodological framework, the following steps are taken:

First, the building blocks of a raster dataset – the pixels – are of equal size. In the example of Figure 2, each pixel is $r \times r$ in size. Therefore, the initial MI for each pixel in a raster dataset is the same and could be obtained by adapting Equation (20):

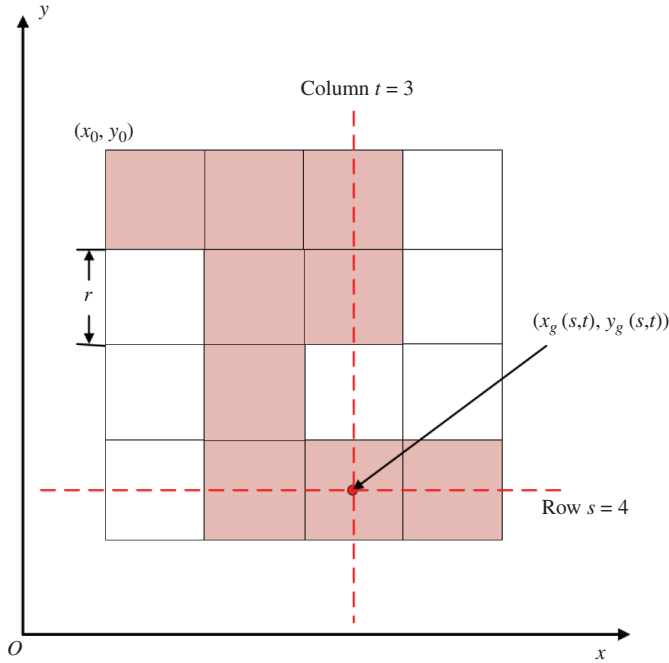


Figure 2. Raster data represented in a projected coordinate reference system (CRS).

$$da = r^2 \tag{33}$$

$$I_{da} = r^2 da / 6 = r^4 / 6 \tag{34}$$

Second, the MI of a shape can be obtained by replacing the integral in Equation (9) with the sum over the pixels that constitute the shape, shown in Equation (34),

$$I_g = \sum_{s,t \text{ where } M(s,t) \neq \text{null}} z_g^2 r^2 \tag{35}$$

To obtain z_g , the centroid of each pixel and the centroid of the entire shape need to be computed. Take the shape (shaded in red) in Figure 2, for example, where the centroid coordinates $(x_g^{s,t}, y_g^{s,t})$ at row s and column t are a function of cell size r , its indices s and t , and the actual coordinates (x_0, y_0) in the upper left corner:

$$x_g^{s,t} = x_0 + c/2 + c(t - 1) \tag{36}$$

$$y_g^{s,t} = y_0 - c/2 - c(s - 1) \tag{37}$$

The centroid for the entire shape can be calculated by averaging the x and y coordinates of all the pixels composing the shape (where $M(s,t) \neq \text{null}$):

$$x_g = \frac{\sum_{\forall s, t \text{ where } M(s,t) \neq \text{null}} x_g^{s,t}}{\sum_{\forall s, t \text{ where } M(s,t) \neq \text{null}} 1} \quad (38)$$

$$y_g = \frac{\sum_{\forall s, t \text{ where } M(s,t) \neq \text{null}} y_g^{s,t}}{\sum_{\forall s, t \text{ where } M(s,t) \neq \text{null}} 1} \quad (39)$$

Given the centroid coordinates of each pixel from Equations (36) and Equations (37), and the centroid coordinates of the entire shape from Equations (38) and Equations (39), z_g , which denotes the Euclidean distance between any pixel centroid and the centroid of the shape, can be easily calculated. Consequently, the MI of the entire shape can be computed from Equation (35). Similarly, when a raster representation is used in a regionalization process, Equations (25)–(28) can be adopted to compute the updated MI when combining two contiguous regions together and Equations (29)–(32) can be adopted for MI computation when a sub-region is removed from a region. Then by applying Equation (11), the compactness index of a changing shape involving a raster representation can be generated.

4. Computer implementation

The proposed method was implemented using the open-source cross-platform programming language Python with the support of Esri's ArcPy package (Esri 2012). Figure 3 shows the object-oriented design of the program, in which five classes (*DataSet*, *MultiPartPolygon*, *Polygon*, *LineSegment*, and *Point*) and their associations are defined. When reading shapes from a dataset, each shape record is cached as an instance of *MultiPartPolygon* class. A *MultiPartPolygon* record may be a single-part polygon, a multi-part polygon, or a polygon with holes. Therefore, the list 'parts' is defined. It contains the variable 'flag' indicating the type of a shape (0 represents the main or a single-part polygon, 1 for the remaining parts in a multi-part polygon, and 2 for a hole) and a variable of the type *Polygon*, which records the actual geographic data that represent each part of a shape. In a *Polygon* class, each polygon (must be single-part) can be represented by a list of its vertices. Each vertex has type *Point*, defined by its x and y coordinates in the CRS (Coordinate Reference System) and documented in the metadata of the dataset. The class *LineSegment* is used when computing the MI of each trapezium formed by the line segments of a polygon.

Figure 4 shows the workflow for computing the MI of shapes with a vector representation. The applications of the above five classes are highlighted at their first occurrences within the whole procedure. The components on the left side are for pre-processing, in which all shapes are read and organized in the data structure defined in Figure 3. The components on the right side of the figure deal with the MI computation for each multi-part polygon in the dataset. The function *combine()* implements Equation (24), when the MIs of all trapezia are adjusted to the polygon's centroid to obtain the MI of the entire polygon about its centroid. A rule needs to be instituted for determining which trapezia fall inside the polygon area and which fall outside. For vertices that are ordered clockwise around a polygon, such as the one shown in Figure 1, the trapezium should be added when $x_{i+1} \geq x_i$ and should be subtracted when $x_{i+1} < x_i$. For 'counterclockwise' ordering of vertices along the boundary of a polygon, the opposite applies. The *isClockwise()* operation in

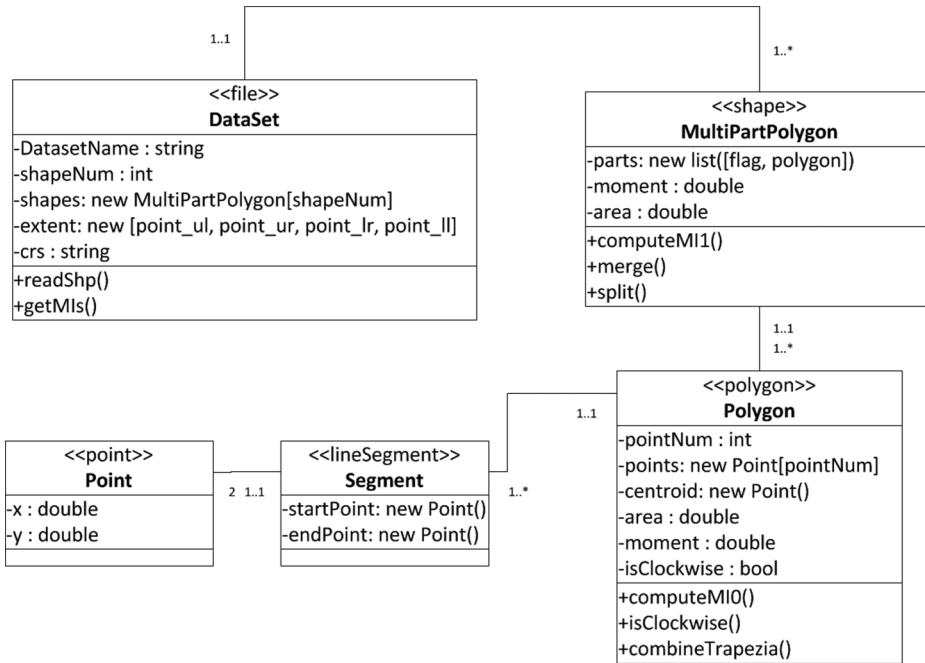


Figure 3. UML design of classes and associations in computer implementation.

the *Polygon* class is used to accomplish this task. In this way, the MI of any regular polygon can be computed.

When it comes to computing the MI of a polygon with more than one part, the *split()* and *merge()* processes are adopted. If the part is a hole, the *split()* function is called to remove the MI of the hole from the shape and the MI introduced by the splitting (Equations (29)–(32)); otherwise, the *merge()* function, which implements Equations (25)–(28), will be called. These two functions could be easily adapted to handle the case of computing the MI of a growing or shrinking region in a regionalization problem.

In handling a raster dataset, a similar procedure can be adopted. In this case, a pixel corresponds to a *Polygon* class, each individual shape corresponds to a *MultiPartPolygon*, and the raster dataset corresponds to the class of *Dataset*. The difference is that only the workflow on the right-hand side of Figure 4 is executed since the MI for each pixel can be easily calculated from Equation (35).

5. Comparing the moment of inertia shape index with the isoperimetric quotient

5.1. Testing the robustness of MI and IPQ shape indices for vector data under positioning uncertainty

Our first test involves calculating the robustness of the proposed MI compactness measure and the popular IPQ approach in handling data with uncertainties. As we know, there will always be some amount of positional error in geospatial data, because exact measurement of location is impossible. Consider a hypothetical study area given in Figure 5a represented by a polygon. We randomly repositioned its vertices to introduce small positioning

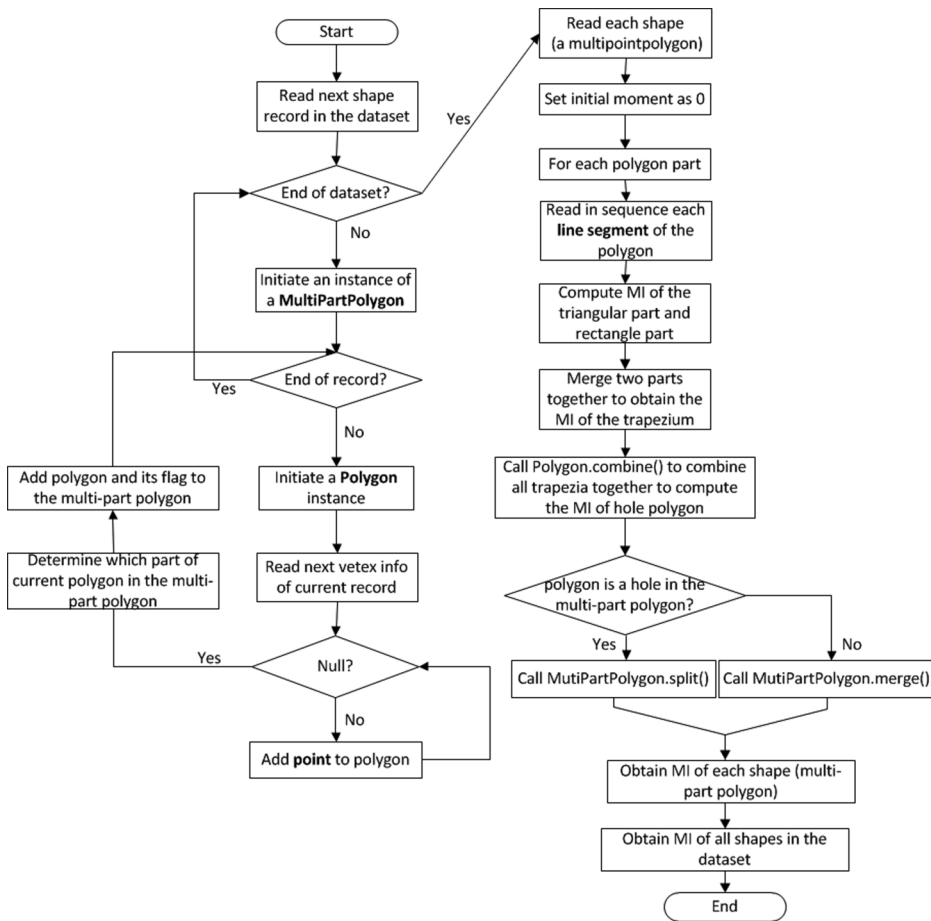


Figure 4. Workflow for computing the MI of shapes.

errors. Table 1 shows the parameters of the experimental settings. For each generated polygon instance, we calculated the MI shape index and the IPQ shape index. This process was repeated n times, and the mean and standard deviation of the MI and IPQ indices were compared. Figure 5a shows the original test shape and all its vertices, and Figure 5b shows the shape before and after distortion. From a visual perspective, we can observe from Figure 5b that this repositioning had little impact on the overall compactness of the shape or area.

Table 2 presents the statistical results associated with 3000 randomly determined instances for each level of positional error buffer size. For each level, the table lists the minimal, maximal, mean, and standard deviation of shape indices for both MI and IPQ. The mean shape indices calculated from the MI approach are almost invariant over the entire range of error buffer sizes. In contrast, the IPQ values vary considerably over the range of levels of error buffer values, from a high of 0.8464 to a low of 0.3474. Given that the shape remains relatively the same over the range of values, the compactness index should have remained relatively constant as well. In this case, the IPQ appears to be too sensitive to issues of positional error, whereas the MI inspired compactness index tolerates positioning errors much better for a digitalized object.

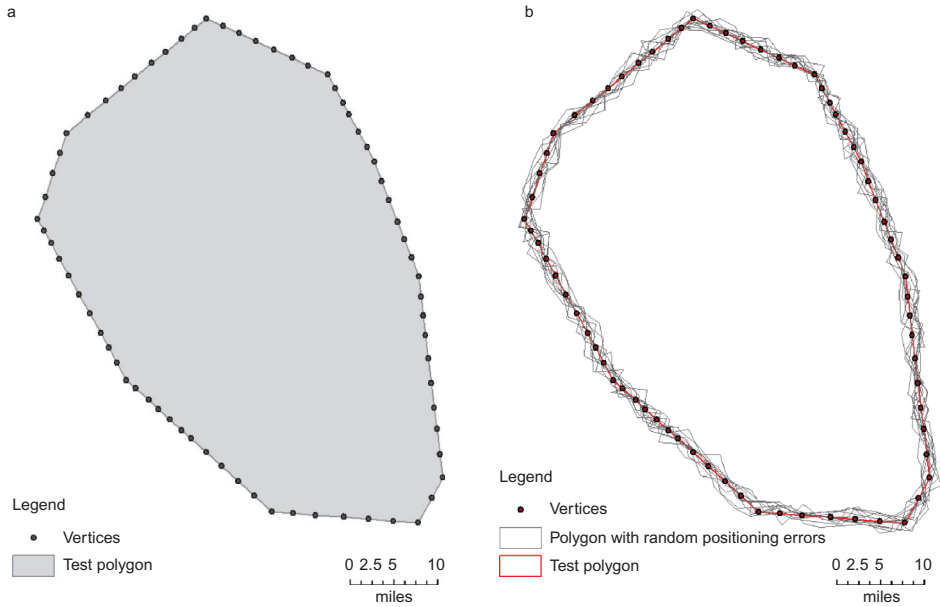


Figure 5. (a) Test polygon and (b) the 10 realizations of polygons with positioning errors ($d = 1$) out of 3000 samples.

Table 1. Parameter settings.

Parameter	Value
Number of vertices of the test polygon	70
Perimeter	58
Area	228
Runs of randomized repositioning n	3000
Error buffer d	[2, 1, 3/4, 1/2, 1/4, 3/16, 1/8, 1/16]

Table 2. Statistical results of shape indices computed from MI and IPQ.

Error buffer, d	MI-moment of inertia				IPQ-isoperimetric quotient			
	Min	Max	Mean	Std dev. (%)	Min	Max	Mean	Std dev. (%)
1/16	0.8754	0.8776	0.8764	0.03	0.8408	0.8506	0.8464	0.14
1/8	0.8739	0.8792	0.8764	0.06	0.8319	0.8531	0.843	0.28
1/4	0.8701	0.8821	0.8761	0.19	0.7809	0.8436	0.8133	0.92
3/8	0.8676	0.8859	0.8759	0.26	0.7452	0.8339	0.7901	1.29
1/2	0.8666	0.8849	0.8759	0.26	0.7355	0.8297	0.79	1.30
3/4	0.8608	0.8879	0.8753	0.40	0.661	0.7833	0.7268	2.02
1	0.8571	0.8915	0.8743	0.54	0.5545	0.734	0.6472	2.64
2	0.8288	0.9018	0.8679	1.12	0.2655	0.4512	0.3474	2.94

5.2. Robustness test of the MI and IPQ shape indices for vector data under shape generalization

Our next experiment involved testing the effects of cartographic generalization on the performance of the MI and IPQ shape indices. Figure 6 shows an initial boundary of Maine

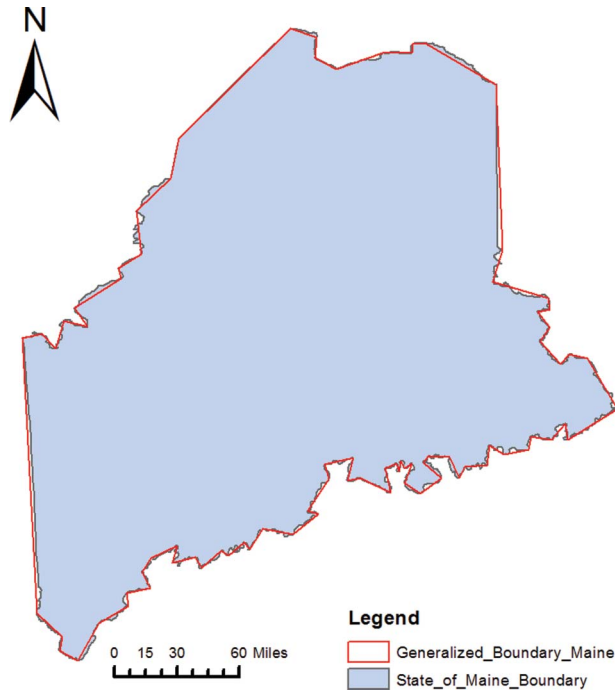


Figure 6. Overlay of original and generalized boundaries of State of Maine.

(excluding islands) and its comparison with a generalized boundary. These shapes have the same general outline, but the outline of the generalized shape is smoother than the original one. The Douglas–Peucker algorithm (Douglas and Peucker 1973) was used to simplify the shape boundary, within tolerance windows from 500 m to 4 km, by 500 m increments. As the tolerance distance increases, the boundary is represented by fewer points, and therefore fewer cartographic details are retained, and the perimeter decreases in length as well. Figure 7 shows the variation in both the MI and IPQ shape indices when the perimeter of Maine is smoothed through line generalization. The perimeter values given along the x -axis were normalized using the initial perimeter length (1979 km). Points closer to the origin represent generalized shapes with larger tolerance distances. We can observe from the figure that IPQ drops monotonically as the perimeter of the Maine boundary increases (as the impact of line generalization decreases), even though the resulting shape remains nearly the same. In contrast, the MI index remains relatively the same across all levels of generalization. We conclude here that the MI index is insensitive to boundary roughness and thus is more robust, in general, for shapes with rugged boundaries.

5.3. Computational efficiency in generating MI index for vector and raster data

In this next experiment, we compared the computational efficiency of a vector computation of MI using integrals and a raster representation using summation for a test area of biological habitat. The tests were conducted on a workstation with Intel Core(TM) i5 2 3.2GHz CPU and 8GB of RAM. Figure 8a shows the hypothetical habitat patch extracted from the habitat of the endangered San Joaquin Kit Fox (SJKF). The habitat area in the

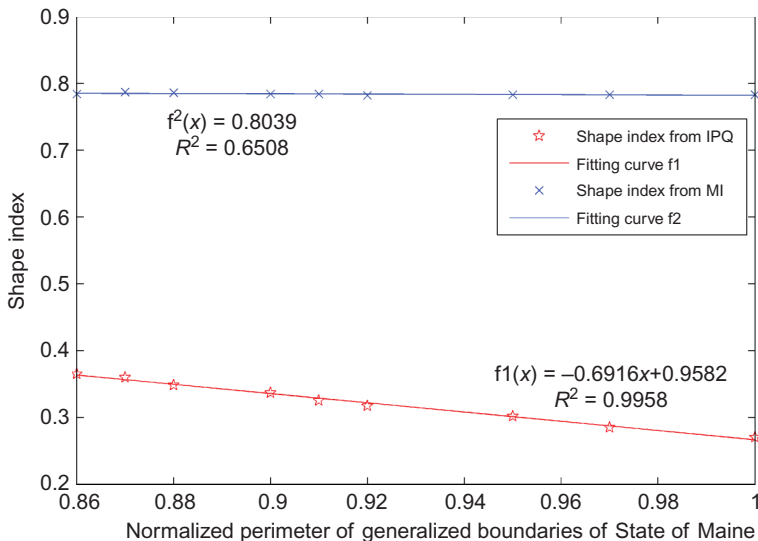


Figure 7. Variation of shape indices from IPQ and MI for generalized boundaries.

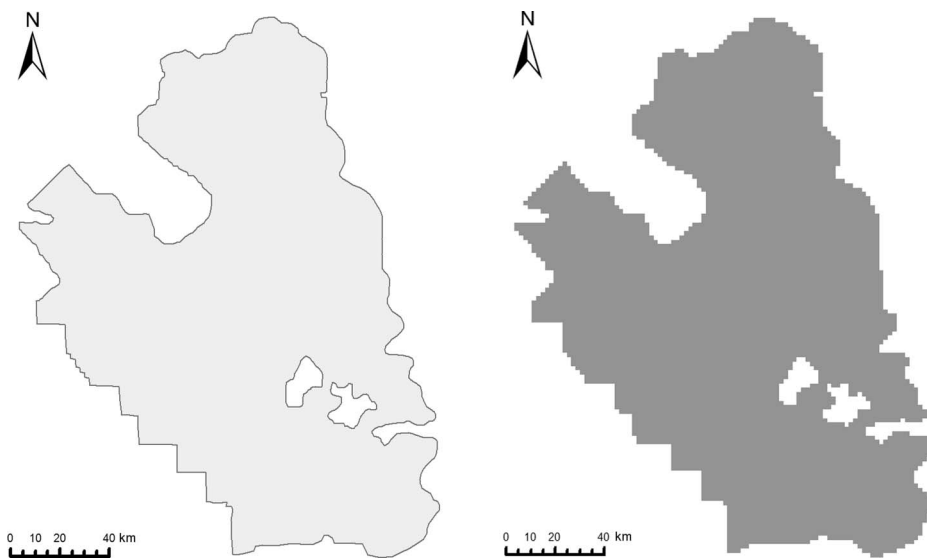


Figure 8. Hypothetical habitat patch (a) and its raster representation with spatial resolution at 1800 m (b).

figure represents areas that lie in three counties (Kings County, Tulare County, and Kern County) of Southern California (CalEPA 2002). The two holes within the patch are agricultural and residential areas considered outside of desired habitat. Figure 8a presents a vector representation of the habitat. In order for making a comparative study, the data in the vector representation were resampled at 10, 30, 90, 180, 270, 360, and 450 m, respectively. Figure 8b shows a raster representation of the same area with a cell size of 1800 m.

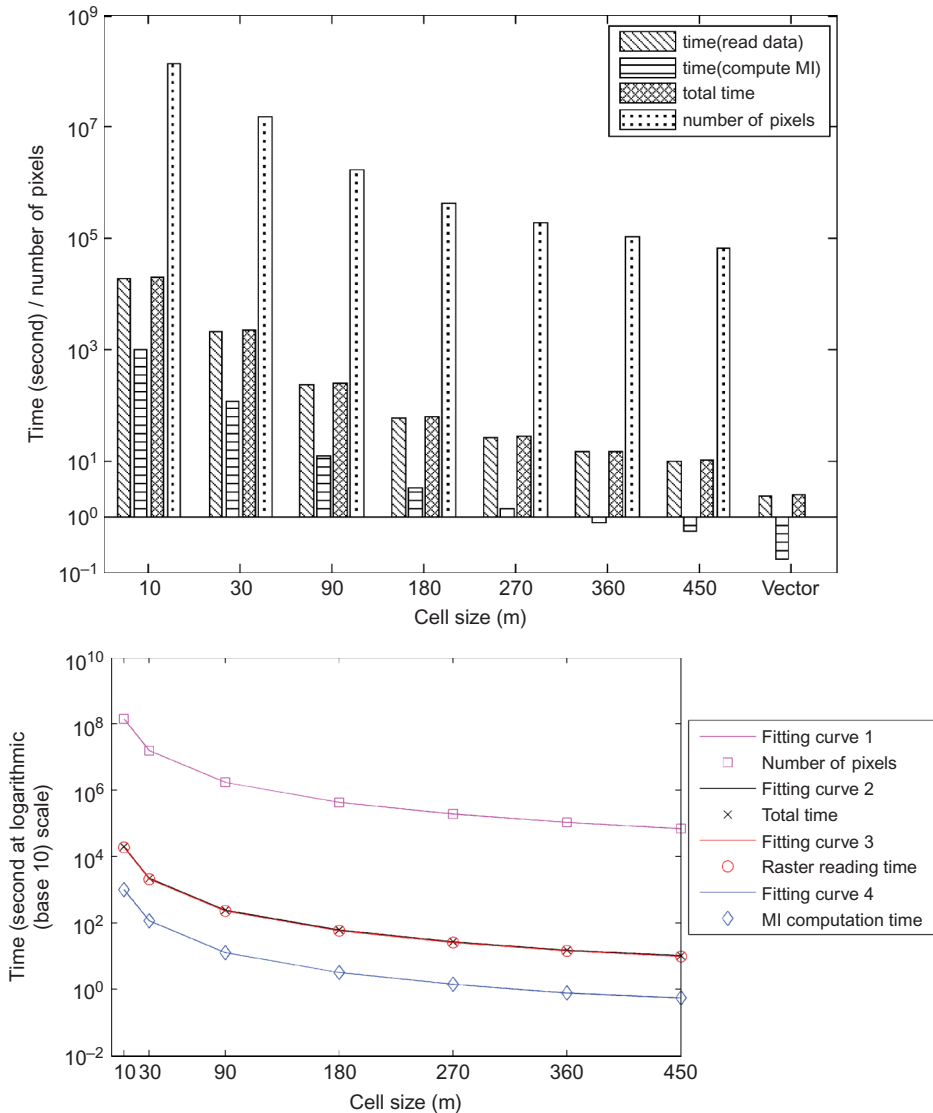


Figure 9. (a) Time efficiency comparison of MI computation for raster and vector data. (b) Regression analysis between computation time and cell sizes.

Figure 9 shows the completion times for the calculation of the MI shape index for the habitat patch depicted in Figure 8 for seven different raster resolutions as well as in vector format. The time required to calculate the MI shape values for raster data can be divided into the time needed to read in the data and the time needed for computing the MI index by merging the MI value of each pixel within the entire shape. Because the MI of each pixel in a raster dataset is the same, there is no need to repeatedly compute it as the pixels are read and processed. Figure 9a shows (1) the time used by each task for computing the MI index from a raster dataset at different cell sizes, (2) the time used for computing the MI of the same shape from the vector dataset, and (3) the number of

pixels involved for each cell size value. From this analysis, one can see that for completing this task, the fastest time for computing the MI compactness index is when using a vector representation. The time needed to read in the dataset dominates the total processing time for both raster and vector models. The actual time used for computing the MI index, for raster data through summation and for vector data through the integral process, after the data are read only takes 5% of the total processing time, suggesting that the proposed method is very computationally efficient. When the raster model is used, the computation time increases dramatically as spatial resolution increases (cell size decreases). This is due to the fact that as the cell size decreases, the total number of pixels used for representing the shape increases by x times (where x equals the square of the ratio between old and new cell sizes). As each pixel acts as a building block for computing the entire MI of a shape, the time consumed will be linearly correlated to the total number of pixels. Therefore, when the size of a cell decreases, the computation time increases significantly. Figure 9b presents a regression analysis between the relationships of total computational time, total number of pixels, total read time, and MI computation time versus the pixel size. The y -axis (representing time) is displayed on a logarithmic scale (using base 10). In each case, R^2 value equaled 0.99. On an average, it takes 1/10,000 of a second to incorporate a single pixel into the MI computation for a raster-based approach. For the vector data model, the time complexity is $O(n)$, where n denotes the number of vertices of a shape.

Therefore, in terms of time efficiency, computing an MI compactness index using a vector model will outperform a raster model. Although the computation of a raster-based MI approach takes much longer than using vector data, it is still decently efficient. For instance, for a shape with 1 million pixels, the total processing time is less than 3 minutes in the current testing environment. Through our experiments, we validated the computational efficiency of the proposed method, due to its quality of being additive.

5.4. Robustness of MI, IPQ, and NDC in handling shapes with holes

In addition to the experiments detailed in Section 5.3, the three popular methods MI (capable of handling both raster and vector data), IPQ (capable of handling vector data), and NDC (capable of handling raster data only) were compared in terms of their performances in measuring the compactness of shapes with holes. The shape in Figure 8 was also used in this experiment. A cursory examination of Figure 8 reveals that the areas of the holes appear to be small enough that the effect they have on shape whether included or not should be quite small. The IPQ compactness index for the region with the two holes is 26% smaller than the IPQ index for the region without holes. This is due to the fact that the IPQ index is based upon both perimeter and area, so the perimeter increases and area decreases when holes are introduced. In comparison, the compactness index drops only 0.3% when the NDC approach is applied to the patch with the two holes as compared to the patch with no holes. This happens because for a large area represented by small cells as shown in Figure 8b, the perimeter is much smaller than the number of cells used to represent the same area. Therefore, the variation in perimeter is insignificant when computing the NDC index. When using the proposed MI approach, the compactness index drops 2% when the two holes are taken into account, suggesting a relatively small but detectable change in the compactness of the general region. This result agrees with our observations. It is important to note that when holes of a shape are considered in computing the compactness index, different shapes may result in identical values. Altogether, one can conclude that the MI

shape index outperforms the IPQ method and is equal to or better than the NDC method in reflecting the actual compactness of shapes with holes.

In summary, our tests have shown that the MI shape index (1) efficiently handles both vector and raster data; (2) is insensitive to positioning errors; (3) tends to be consistent across data represented at varying resolutions; (4) easily handles shapes with holes; and (5) is robust in handling irregular boundaries. Our tests of the conventionally accepted standard, IPQ, demonstrated weaknesses among virtually all of our tests (roughness, positioning uncertainty, holes, and resolution). Adopting an MI shape measure as a standard of shape measurement has been hampered by the lack of an efficient, computationally simple method of computing the moment of inertia. The methods (both the vector and raster) presented in Sections 3 and 4 have eliminated this major hurdle. Consequently, the MI shape approach should be adopted in practice.

6. Case study: a regionalization problem

In this section, we apply the MI approach to a compactness-driven, multi-constraint regionalization problem that requires the generation of a set of compact regions that form the basic spatial units of a microeconomic model. Our goal was to aggregate the 4109 transportation analysis zones (TAZs) in six counties of Southern California (Los Angeles, Riverside, San Bernardino, Orange, Imperial, and Ventura, as shown in Figure 10) into approximately 100 regions, the maximum number considered computationally feasible for subsequent work in the microeconomic simulation of the study area. Our objective is to maximize the overall compactness of the generated regions while at the same time satisfying the following constraints: (1) each region must be spatially contiguous, (2) the boundaries of regions must not cross major physiographic features and county boundaries,

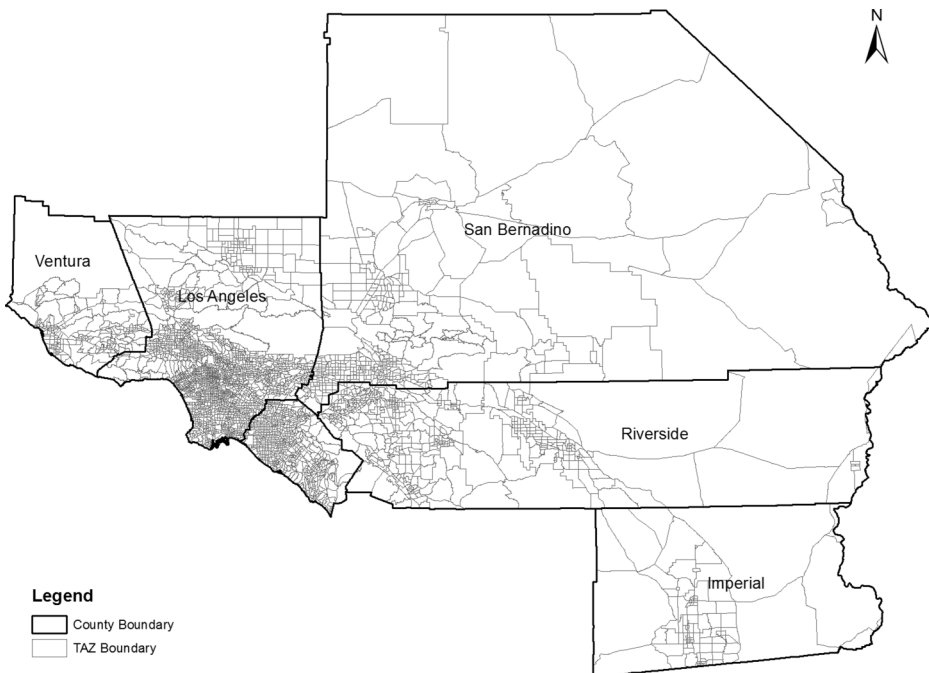


Figure 10. TAZ boundaries in the study area.

and (3) the intra-zonal traffic within a generated region must be smaller than a certain percentage of all traffic generated by that region. Although we do not give a mathematical formulation here, this problem can be defined as a nonlinear integer-programming problem. It is considered to be of a size and model type that is difficult to solve optimally for even very small problems. Because our problem involved over 4000 ‘atomic’ units, we were forced to consider a heuristic approach.

We developed a greedy-based heuristic algorithm for the zoning process. Briefly, it includes four phases, outlined as follows. (1) Initialization: each region is originally assigned a ‘seed’ TAZ as a starting point. (2) Dealing phase: each region is allowed to grow initially to a viable size. Similar to dealing cards in a card game, each region is assigned a TAZ that touches its border and helps keep it compact and maintain constraints. Dealing is continued until all regions achieve a minimal size. (3) Randomized Greedy growth: for each region, identify the candidate TAZ not yet assigned to any region that would improve the objective the most (while maintaining constraints) if added to that region. Considering all regions, identify the top three regions that will improve the most if allowed to add their candidate TAZs. Select at random one of these three regions and add its best candidate TAZ to that region. Repeat this step until each TAZ has been assigned to one of the 100 regions. (4) Adaptive Search Procedure: if moving a TAZ on a region boundary to another region will improve the objective function and not violate the constraints, then this TAZ is moved. This process is repeated until no further improvement can be found.

To demonstrate how easily the proposed MI computation can be applied to such a regionalization problem, two simplified scenarios are given. Figure 11 shows a partial region P_1 at state j , its three adjacent TAZs – the atomic units (A_1 , A_2 , and A_3), and their centroids (in black). To decide which TAZ to aggregate with region P_1 , its MI is computed after combining the three TAZs according to Equations (25)–(28). Then by substituting

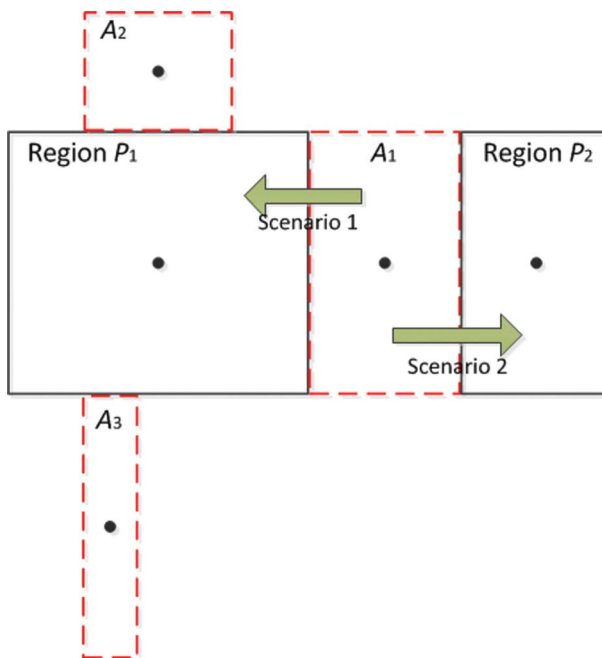


Figure 11. An example of region growth.

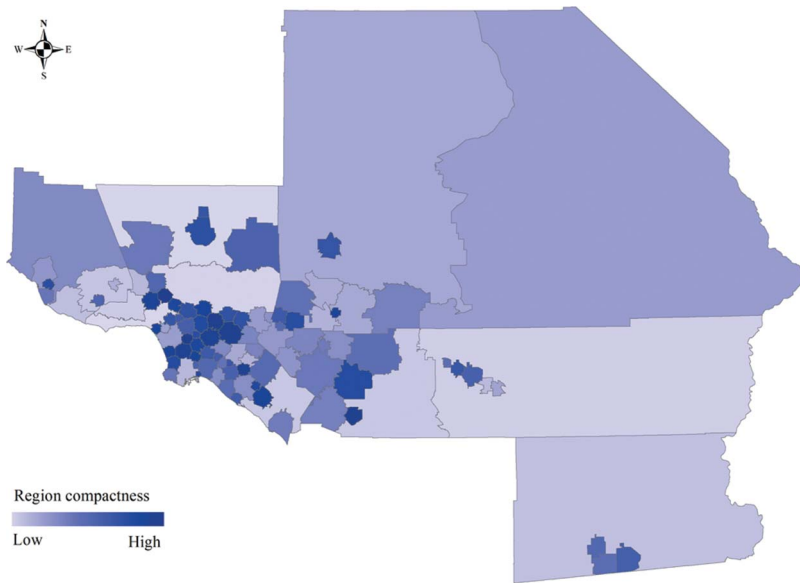


Figure 12. The best zoning solution out of 333 heuristic trails, using the MI shape index as the compactness measure.

the MI values in Equation (11), the new shape index of P_1 in each case can be obtained. Given that the improvement of compactness for P_1 made by adding A_1 is larger than when adding A_3 , A_1 will be chosen as the candidate TAZ to grow region P_1 (the TAZ that introduces the maximal compactness improvement will be chosen as the candidate to grow a region). The second scenario takes place in the adaptive search phase. Suppose that (1) region P_1 has now included A_1 ; (2) A_2 and A_3 have been assigned to other regions; and (3) there is another region P_2 which is adjacent to P_1 along a common edge on A_1 . At this point, the variation of overall compactness introduced by moving A_1 from P_1 to P_2 should be tested. This involves calculating the change of compactness for P_1 due to disaggregation of A_1 through the application of Equations (29)–(32), as well as that of P_1 with the aggregation of A_1 through the application of Equations (25)–(28). If the sum of the variation is positive, it indicates that this move will increase the overall compactness, so A_1 should be moved. Because the centroid, area, and MI of each TAZ (A_1 , A_2 , and A_3) were pre-calculated using Equations (12)–(24) and the computation of the new MI of a region after (dis)aggregation only requires a few ‘add’ operations rather than being dependent on the number of atomic units of a region, the time complexity is only $O(1)$ for computing a region’s compactness index as its shape changes. This demonstrates that the integration of the proposed compactness measure into a regionalization problem can be very easily and efficiently accomplished.

Figure 12 shows the best zoning plan obtained by applying the MI-based compactness measure as the objective. Visually, the regions in Figure 12 are mostly round and close to round, except for those restricted by the political and physiographical boundaries. Statistically, of the 100 regions generated, 91% achieve compactness over 0.8, 66 of the 100 achieve compactness over 0.9, and only 9 of them have compactness below 0.8. This demonstrates the good performance of the proposed MI approach in generating compact zones in a regionalization problem.

7. Discussion and conclusion

Adopting an MI index as a standard for shape measurement has been hampered by the lack of an efficient, computationally simple method of computing the moment of inertia. Previous discussions remained at the conceptual level (Kaiser 1966, Young 1988) or focused on the implementation of only a single shape's compactness measure (Zhang *et al.* 2006). In this article, we proposed a clear mathematical definition and computer implementation of a trapezium-based approach for computing moment of inertia and the corresponding compactness index based upon it. This approach has the advantage of uniquely determining the compactness value, in comparison with the triangular approach proposed by Massam and Goodchild (1971). Through successive experiments in Section 5, we demonstrated that measuring compactness with the proposed MI shape index has clear advantages over the commonly used IPQ. Moreover, we not only discussed the MI computation for vector data, we also presented a specialized form in which it can be applied to a raster data model. We successfully integrated this measure into a large and practical regionalization problem to demonstrate its easy extendibility and integrity. This article makes a major contribution to geographic analysis through the development of a robust, additive, computationally efficient, and easy-to-integrate compactness measure. It also proposes that an MI shape index should be considered as a standard method for measuring compactness.

Though the discussion in this article has been focused on measurements based on pure geometry, the MI approach is easily extended to applications measuring compactness weighted by the distribution of a property such as population, which is a feature that is not supported by any of the other methods discussed. In a vector model, we could assume that each basic spatial unit (a single shape) had a uniform density ρ , and by weighting each element of area dA in Equation (7) by ρ , a density-weighted shape index can be obtained. When it is desirable to investigate the property at a finer level of detail, the shift can be made to a raster representation and the shape index can be measured by a weighted summation of pixels for that property. This will be the direction taken in our future research in order to extend the methodological framework. We will also promote and broaden the application of the proposed compactness measure to enhance the ability to precisely identify compact spatial clusters, as needed in multiple scientific fields such as spatial epidemiology and criminology.

Acknowledgements

The application to Southern California is funded by the University of California's Office of the President and is being carried out as a collaboration between researchers at the University of California's Riverside, Berkeley, and Santa Barbara campuses and at the University at Buffalo. The cooperation of collaborators at Harvard University and the staff of the Southern California Association of Governments in providing access to data is also acknowledged.

References

- Angel, S., Parent, J., and Civco, D. L., 2010. Ten compactness properties of circles: measuring shape in geography. *Canadian Geographer-Geographe Canadien*, 54 (4), 441–461.
- Bachi, R., 1999. *New methods of geostatistical analysis and graphical presentation: distributions of populations over territories*, 1 ed. New York, NY: Springer.
- Bardossy, A. and Schmidt, F., 2002. GIS approach to scale issues of perimeter-based shape indices for drainage basins. *Hydrological Sciences Journal (Journal Des Sciences Hydrologiques)*, 47 (6), 931–942.
- Bottema, M.J., 2000. Circularity of objects in images. *International Conference on Acoustic, Speech and Signal Processing*, Istanbul, 2247–2250.
- Bribiesca, E., 1997. Measuring 2-D shape compactness using the contact perimeter. *Computers & Mathematics with Applications*, 33 (11), 1–9.

- CalEPA, 2002. San Joaquin Kit Fox (*Vulpes macrotis mutica*) [online]. Available from: <http://www.cdpr.ca.gov/docs/endspec/espdfs/sjkfall.pdf> [Accessed 01 Jun 2012].
- Chandra, S., Chhetri, P., and Corcoran, J., 2009. Spatial patterns of urban compactness in Melbourne: an urban myth or a reality. In: B. Ostendorf, P. Baldock, D. Bruce, M. Burdett and P. Corcoran, eds. *Proceedings of the Surveying and Spatial Sciences Institute Biennial International Conference*, Adelaide, Australia, 231–242.
- Christaller, W., 1968. Wie ich zu der Theorie der zentralen Orte gekommen bin. *Geographische Zeitschrift*, 56 (2), 88–101.
- Cole, J.P., 1964. Study of major and minor civil divisions in political geography. *The 20th International Geographical Congress*, London.
- Datta, D., Malczewski, J., and Figueira, J.R., 2012. Spatial aggregation and compactness of census areas with a multiobjective genetic algorithm: a case study in Canada. *Environment and Planning B-Planning & Design*, 39 (2), 376–392.
- Douglas, D. H. and Peucker, T. K., 1973. Algorithms for the reduction of the number of points required to represent a digitized line or its caricature. *The Canadian Cartographer*, 10 (2), 112–122.
- Duque, J.C., Ramos, R., and Surinach, J., 2007. Supervised regionalization methods: a survey. *International Regional Science Review*, 30 (3), 195–220.
- Eason, P., 1992. Optimization of territory shape in heterogeneous habitats – a field-study of the red-capped cardinal (*Paroaria-Gularis*). *Journal of Animal Ecology*, 61 (2), 411–424.
- Edwards, J. D., Riley, K. J., and Eakins, J. P., 2003. A visual comparison of shape descriptors using multi-dimensional scaling. *Computer Analysis of Images and Patterns, Proceedings*, 2756, 393–401.
- Esri, 2012. *Geoprocessing with Python* [online]. Available from: http://help.arcgis.com/en/arcgisdesktop/10.0/help/index.html#/Importing_ArcPy/002z00000008000000/ [Accessed 01 Jun 2012].
- Friedenberg, J., 2012. Aesthetic judgment of triangular shape: compactness and not the golden ratio determines perceived attractiveness. *i-Perception*, 3, 163–175.
- Frolov, Y.S., 1975. Measuring shape of geographical phenomena - history of issues. *Soviet Geography Review and Translation*, 16 (10), 676–687.
- Fryer, R.G. Jr and Holdeen, R.T., 2007. *Measuring the compactness of political districting plans* [online]. Available from: <http://www.nber.org/papers/w13456> [Accessed June-01 2012].
- Gibbs, J.P., 1961. A method for comparing the spatial shapes of urban units. In: J.P. Gibbs, ed. *Urban research methods*. Princeton, NJ: Van Nostrand, 99–106.
- Gillman, R., 2002. Geometry and gerrymandering. *Math Horizons*, 10 (1), 10–13.
- Goodchild, M.F., 1996. Generalization, uncertainty, and error modeling. In: *Proceedings of GIS/LIS 96*. Bethesda, MD: American Society for Photogrammetry and Remote Sensing, 765–774.
- Hauert, J.H. and Wolff, A., 2010. Area aggregation in map generalisation by mixed-integer programming. *International Journal of Geographical Information Science*, 24 (12), 1871–1897.
- Horn, D.L., Hampton, C.R., and Vandenberg, A.J., 1993. Practical application of district compactness. *Political Geography*, 12 (2), 103–120.
- Kaiser, H.F., 1966. An objective method for establishing legislative districts. *Midwest Journal of Political Science*, 10 (2), 200–213.
- Kim, C.E. and Anderson, T.A., 1984. Digital disks and a digital compactness measured. In: *Proceedings of the sixteenth annual ACM symposium on theory of computing*. New York, NY: ACM Press, 117–124.
- Landau, L.D. and Lifschitz, E.M., 1984. *Electrodynamics of continuous media*. 2nd ed. Oxford, England: Pergamon Press, 460 pp.
- Maceachren, A.M., 1985. Compactness of geographic shape – comparison and evaluation of measures. *Geografiska Annaler Series B-Human Geography*, 67 (1), 53–67.
- Martin, D., Nolan, A., and Tranmer, M. 2001. The application of zone-design methodology in the 2001 UK census. *Environment and Planning A*, 33 (11), 1949–1962.
- Massam, B.H. and Goodchild, M.F., 1971. Temporal trends in the spatial organization of a service agency. *Canadian Geographer*, 15, 193–206.
- Miller, V.C., 1953. *A quantitative geomorphic study of the drainage basin characteristics in the Clinch Mountain area, Virginia and Tennessee*. New York: Columbia University Department of Geology Technical Report, No. 3.

- Openshaw, S., 1977. Geographical solution to scale and aggregation problems in region-building, partitioning and spatial modeling. *Transactions of the Institute of British Geographers*, 2 (4), 459–472.
- Openshaw, S., 1978. Empirical-study of some zone-design criteria. *Environment and Planning A*, 10 (7), 781–794.
- Openshaw, S. and Rao, L., 1995. Algorithms for reengineering 1991 census geography. *Environment and Planning A*, 27, 425–425.
- Osserman, R., 1978. Isoperimetric inequality. *Bulletin of the American Mathematical Society*, 84 (6), 1182–1238.
- Ovsjanikov, M., et al., 2009 Year. ShapeGoogle: a computer vision approach to invariant shape retrieval. In: *Proceedings of second workshop on nonrigid shape analysis and deformable image alignment*. Kyoto, Japan: IEEE Publisher.
- Richardson, L.F., 1961. A note: measuring compactness as a requirement of legislative apportionment. *Mid-west Journal of Political Science*, 5, 70–74.
- Rinder, D., Armstrong, A., and Openshaw, S., 1988. The domesday machine: a nationwide geographical information system. *Geographical Journal*, 154 (1), 56–68.
- Santiago, R.S. and Bribiesca, E., 2009. State of the art of compactness and circularity measures. *International Mathematical Forum*, 4 (27), 1305–1335.
- Tobler, W.R., 1970. Computer movie simulating urban growth in Detroit region. *Economic Geography*, 46 (2), 234–240.
- Weaver, J.B. and Hess, S.W., 1963. A procedure for nonpartisan districting: development of computer techniques. *The Yale Law Journal*, 72, 288–308.
- Wentz, E.A., 2000. A shape definition for geographic applications based on edge, elongation, and perforation. *Geographical Analysis*, 32 (2), 95–112.
- Wentz, L., 1997. Shape analysis in GIS. *AutoCarto*, 5, 204–213.
- Young, H.P., 1988. Measuring the compactness of legislative districts. *Legislative Studies Quarterly*, 13 (1), 105–115.
- Zhao, Z.Q. and Stough, R.R., 2005. Measuring similarity among various shapes based on geometric matching. *Geographical Analysis*, 37 (4), 410–422.
- Zhang, S.Q., et al., 2006. Vector analysis theory on landscape pattern (vatlp). *Ecological Modelling*, 193 (3–4), 492–502.